



HAL
open science

Overexpression of an $\alpha 1H$ (Cav3.2) T-type Calcium Channel during Neuroendocrine Differentiation of Human Prostate Cancer Cells

Pascal Mariot, Karine Vanoverberghe, Nathalie Lalevée, Michel F Rossier,
Natalia Prevarskaya

► **To cite this version:**

Pascal Mariot, Karine Vanoverberghe, Nathalie Lalevée, Michel F Rossier, Natalia Prevarskaya. Overexpression of an $\alpha 1H$ (Cav3.2) T-type Calcium Channel during Neuroendocrine Differentiation of Human Prostate Cancer Cells. *Journal of Biological Chemistry*, 2002, 277 (13), pp.10824-10833. 10.1074/jbc.m108754200 . hal-04210287

HAL Id: hal-04210287

<https://hal.science/hal-04210287>

Submitted on 18 Sep 2023

HAL is a multi-disciplinary open access archive for the deposit and dissemination of scientific research documents, whether they are published or not. The documents may come from teaching and research institutions in France or abroad, or from public or private research centers.

L'archive ouverte pluridisciplinaire **HAL**, est destinée au dépôt et à la diffusion de documents scientifiques de niveau recherche, publiés ou non, émanant des établissements d'enseignement et de recherche français ou étrangers, des laboratoires publics ou privés.

Overexpression of an α_{1H} ($Ca_v3.2$) T-type Calcium Channel during Neuroendocrine Differentiation of Human Prostate Cancer Cells*

Received for publication, September 11, 2001, and in revised form, January 14, 2002
Published, JBC Papers in Press, January 17, 2002, DOI 10.1074/jbc.M108754200

Pascal Mariot^{‡§}, Karine Vanoverberghe[‡], Nathalie Lalevée[¶], Michel F. Rossier^{¶||},
and Natalia Prevarskaya[‡]

From the [‡]Laboratoire de Physiologie Cellulaire, INSERM EPI9938, Bâtiment SN3, Université des Sciences et Technologies de Lille, 59655 Villeneuve d'Ascq Cédex, France and the [¶]Division of Endocrinology & Diabetology, Department of Internal Medicine, ^{||}Laboratory of Clinical Chemistry, Department of Pathology, University Hospital, CH-1211 Geneva 14, Switzerland

Neuroendocrine differentiation of prostate epithelial cells is usually associated with an increased aggressivity and invasiveness of prostate tumors and a poor prognosis. However, the molecular mechanisms involved in this process remain poorly understood. We have investigated the possible expression of voltage-gated calcium channels in human prostate cancer epithelial LNCaP cells and their modulation during neuroendocrine differentiation. A small proportion of undifferentiated LNCaP cells displayed a voltage-dependent calcium current. This proportion and the calcium current density were significantly increased during neuroendocrine differentiation induced by long-term treatments with cyclic AMP permeant analogs or with a steroid-reduced culture medium. Biophysical and pharmacological properties of this calcium current suggest that it is carried by low-voltage activated T-type calcium channels. Reverse transcriptase-PCR experiments demonstrated that only a single type of LVA calcium channel mRNA, an α_{1H} calcium channel mRNA, is expressed in LNCaP cells. Quantitative real-time reverse transcriptase-PCR revealed that α_{1H} mRNA was overexpressed during neuroendocrine differentiation. Finally, we show that this calcium channel promotes basal calcium entry at resting membrane potential and may facilitate neurite lengthening. This voltage-dependent calcium channel could be involved in the stimulation of mitogenic factor secretion and could therefore be a target for future therapeutic strategies.

Prostate cancer is a slowly evolutive cancer which, in the first stages, is dependent on androgens. Treatments designed to kill the tumors, based on androgen depletion, become eventually ineffective, this being probably due to the selection of resistant cells. One hypothesis is that androgen-insensitive cells resistant to anti-androgen therapies would be neuroendocrine cells lacking the androgen receptor (1). Extensive and focal neuroendocrine features, determined by cell immunore-

activity to different neuronal markers (neuron-specific enolase (NSE),¹ chromogranin A, synaptophysin), are evidenced in most prostate carcinoma in their late stages (for review, see Refs. 2 and 3). This focal neuroendocrine differentiation is characterized by the presence of dispersed clusters of neuroendocrine cells in a neighboring of non-neuroendocrine dividing cells (1) and is usually associated with an increased aggressivity and invasiveness of the tumors and a poor prognosis (4). Neuroendocrine cells do not proliferate (1) but could be involved in prostate cancer relapse by secreting mitogenic autocrine/paracrine factors like bombesin, calcitonin, and parathyroid hormone-related peptides in their vicinity (3). This could in turn promote either the proliferation of adjacent epithelial cells or their differentiation toward a neuroendocrine phenotype (2). Altogether, these autocrine/paracrine actions could lead to the uncontrolled growth of the prostate.

Some of the signals involved in neuroendocrine differentiation of the prostatic epithelium have been unraveled. Activation of membrane receptors coupled to adenylyl cyclase which leads to an increase in cytosolic cyclic AMP, as well as interleukins 1 and 6 induce the expression of neuroendocrine markers like NSE, secretory granules, and neurite extension (5–9). The stimulation of neuroendocrine differentiation by interleukin 6 has been shown to involve the induction of cyclin-dependent kinase inhibitor p27^{Kip1} (7), as well as the tyrosine phosphorylation of epithelial and endothelial tyrosine kinase Etk/Bmx through the activation of phosphatidylinositol 3'-kinase (6). Steroid removal from the culture medium was also shown to induce neuroendocrine differentiation (10, 11).

Calcium entry through voltage-gated calcium channels is reported to be involved in differentiation and neurite outgrowth in other cells (12–15). It has been shown, for example, in the pheochromocytoma cell line (PC12 cells) that neuroendocrine differentiation is accompanied by an increased expression of voltage-dependent channels like low-voltage activated (LVA) (12) and high-voltage activated (HVA) calcium channels (14, 16). To our knowledge no functional voltage-dependent calcium channels have been clearly demonstrated in prostate cancer cells. We have investigated in this study the possible expression of voltage-gated calcium channels in human prostate cancer LNCaP cells and their modulation during neuroendocrine differentiation induced by increasing cytosolic cAMP or by reducing steroids in the culture medium. We show that a

* This work was supported by the INSERM, Ligue Nationale contre le Cancer, Association pour la Recherche contre le Cancer, Fondation pour la Recherche Médicale, and Swiss National Science Foundation Grant 32-58948.99 (to M. F. R. and N. L.). The costs of publication of this article were defrayed in part by the payment of page charges. This article must therefore be hereby marked "advertisement" in accordance with 18 U.S.C. Section 1734 solely to indicate this fact.

§ To whom correspondence should be addressed: Laboratoire de Physiologie Cellulaire, INSERM EPI9938, Bâtiment SN3, Université des Sciences et Technologies de Lille, 59655 Villeneuve d'Ascq Cédex, France. Tel.: 33-3-20-43-40-77; Fax: 33-3-20-43-40-66; E-mail: Pascal.Mariot@univ-lille1.fr.

¹ The abbreviations used are: NSE, neuron-specific enolase; LVA, low-voltage activated; HVA, high-voltage activated; RT, reverse transcriptase; IBMX, isobutylmethylxanthine; GAPDH, glyceraldehyde-3-phosphate dehydrogenase; $[Ca^{2+}]_i$, intracellular Ca^{2+} ; Bt₂cAMP, dibutyryl cAMP.

small proportion of LNCaP cells displays an inward calcium current of weak amplitude and that this proportion and the calcium current density are increased during neuroendocrine differentiation. Biophysical and pharmacological properties of this calcium current show that it is carried by a LVA T-type calcium channel. RT-PCR experiments demonstrate that only an α_{1H} voltage-dependent calcium channel mRNA is expressed in LNCaP cells. Quantitative real-time RT-PCR reveals that α_{1H} mRNA is overexpressed during neuroendocrine differentiation induced by various stimuli increasing cytosolic cAMP. Finally, our results suggest that although they are not involved in triggering neurite elongation, T-type calcium channels participate to a "window" calcium current active at resting membrane potential and may be implicated in facilitating the extension of neuritic processes. In addition, we propose that this voltage-dependent calcium channel could participate to the stimulation of mitogenic factors secretion by neuroendocrine prostate cells and could therefore be a target for future therapeutic strategies.

EXPERIMENTAL PROCEDURES

Cell Culture and Treatments

LNCaP cells were purchased from the American Type Culture Collection and grown as recommended in RPMI 1640 (Biowhittaker, Fontenay sous Bois, France) supplemented with 10% fetal bovine serum (Seromed, Poly-Labo, Strasbourg, France) and 5 mM L-glutamine (Sigma, L'Isle d'Abeau, France). Cells were routinely grown in 50-ml flasks (Nunc, Poly-Labo) in a humidified atmosphere at 37 °C (95% air, 5% CO₂). To study the role of steroids in the expression of voltage-dependent calcium channels, cells were grown in phenol red-free RPMI 1640 supplemented with 10% charcoal-stripped fetal bovine serum (culture medium thereafter referred to as steroid-reduced medium). For electrophysiological studies, cells were subcultured in Petri dishes (Nunc) using trypsin. The culture medium was then changed every 3 days. Five days after trypsinization, the treatment was initiated and the culture medium containing the treatments (Bt₂cAMP, IBMX) was changed every day. Cells were then tested within 8 days.

Western Blot Analysis

Following treatments, LNCaP cells were lysed in an ice-cold homogenizing buffer (pH 7.4) containing 20 mM HEPES, 50 mM NaCl, 0.5% Nonidet P-40 (v/v), 1 mM EGTA, 10 mM EDTA, 1 mM phenylmethanesulfonyl fluoride, 2 μ g/ml aprotinin, 2 μ g/ml pepstatin A, and 10 μ g/ml leupeptin. The homogenates were cleared by a centrifugation at 900 \times g for 10 min and the protein content in the supernatants was determined using a Bradford assay. 50 μ g of total proteins of each sample were analyzed on a 10% SDS-polyacrylamide gel electrophoresis. After transfer, the blots were blocked in 5% non-fat dry milk in TBST (15 mM Tris buffer (pH 8), 140 mM NaCl, 0.05% Tween 20) before the mouse anti-NSE monoclonal antibody (1/100, M0873 DAKO) was added in TBST-3% non-fat dry milk for 1 h at room temperature. After washing, blots were incubated for 1 h with an horseradish peroxidase-linked secondary antibody (1/5000, Zymed Laboratories Inc., San Francisco, CA) and processed for chemiluminescent detection using Supersignal West Pico chemiluminescent substrate (Pierce, Chemical Co., Rockford, IL) according to the manufacturer's instructions. The blots were then exposed to X-Omat AR films (Eastman Kodak Co., Rochester, NY).

Qualitative and Quantitative RT-PCR

RNA Extraction—Total RNA isolation from 5 million cells in culture was performed using the RNeasy™ Total RNA isolation System kit (Qiagen AG, Basel, Switzerland), as indicated in the manufacturer's instructions. Dry RNA pellets were dissolved in nuclease-free water and stored frozen at a concentration of 500 ng/ μ l.

RT-PCR Procedure—Conventional RT-PCR was performed using the "GeneAmp™ Gold RNA PCR Reagent Kit" from PE-Biosystems following manufacturer's instructions. Briefly, first strand cDNA was generated by loading 300 ng of extracted RNA in the master mixture (50 μ l) containing 500 nM specific primers for calcium channels (see Table I) and other reagents, as specified by the manufacturer. GAPDH (glyceraldehyde-3-phosphate dehydrogenase) transcripts were reverse transcribed and analyzed in parallel to evaluate RNA integrity. Reverse transcription was achieved by incubation at 42 °C for 12 min. A 10-min denaturation step at 95 °C then preceded 32 PCR cycles according to

the following protocol: denaturation at 94 °C (20 s), annealing/elongation at 62 °C (1 min), and a final elongation step at 72 °C (7 min). Amplified fragments were then resolved on a 2% agarose gel.

Quantification by Real-time RT-PCR on LightCycler™—A one-step conventional RT-PCR protocol has been adapted for the LightCycler (Roche Molecular Diagnostics AG, Rotkreuz, Switzerland). Individual glass capillaries were filled with a solution containing 18 μ l of RT-PCR mixture and 2 μ l of total RNA template (250 ng). The reaction mixture was composed of primer oligonucleotides (250 nM), Mn(OAc)₂ (3.5 mM), and LightCycler RNA Master SYBR Green I, itself containing reaction buffer, dNTP, Tth DNA polymerase, and SYBR Green I dye at concentrations optimized by the manufacturer. The reverse transcription of the RNA template lasted 20 min at 61 °C and was followed by a 2-min denaturation of cDNA at 95 °C. The amplification of target cDNA was then performed for 45 cycles according to the following steps: denaturation, 95 °C (5 s); annealing, 54 °C (5 s); and elongation, 72 °C (8 s). The SYBR Green fluorescence was measured after each elongation step. At the end of the PCR, a melting curve analysis was performed by gradually increasing temperature from 60 to 95 °C (0.1 °C/s). Moreover, at the end of experiments, RT-PCR products were removed from capillaries and analyzed by gel electrophoresis to confirm the presence and assess the purity of the amplicons of interest.

After PCR was completed, the SYBR Green fluorescent signal was analyzed and converted into a relative number of copies of target molecules. For this purpose, the results of a series of standards prepared by successive dilutions and plotted against the logarithm of the concentration were used to estimate the relative amount of specific mRNA initially present in the various samples. Each sample was analyzed in triplicate.

Recording Solutions

Bath medium used for calcium imaging or current-clamp experiments consisted in Hank's balanced salt solution containing 142 mM NaCl, 5.6 mM KCl, 1 mM MgCl₂, 2 mM CaCl₂, 0.34 mM Na₂HPO₄, 0.44 mM KH₂PO₄, 10 mM HEPES, and 5.6 mM glucose. For measuring calcium currents in patch-clamp experiments, the external buffer contained 142 mM NaCl, 1 mM MgCl₂, 10 mM HEPES, 5.6 mM glucose, 10 mM TEA-Cl (tetra-ethyl ammonium chloride), and 10 mM CaCl₂ or BaCl₂. All the data shown in this study were obtained with a bath medium containing 10 mM BaCl₂. The osmolality and pH of external buffers were adjusted to 310 mOsm liter⁻¹ and 7.4, respectively.

For current-clamp experiments, the pipette solution contained 140 mM K-glutamate, 1 mM EGTA, 1 mM MgCl₂, 5 mM HEPES. For voltage-dependent calcium current studies, recording pipettes were filled with a solution containing 140 mM n-methylglucamine, 110 mM L-glutamic acid, 30 mM HCl, 5 mM HEPES, 1 mM MgCl₂, 1 mM EGTA. Osmolality and pH were adjusted to 290 mOsm liter⁻¹ and 7.2, respectively.

Electrophysiological Recordings

Patch-clamp recordings were performed in the whole cell configuration (17) using a RK-300 patch-clamp amplifier (Biologic, Grenoble, France). The patch-clamp amplifier was driven by Pulse 8.30 software (HEKA Elektronik, Lambrecht, Germany). Membrane currents were digitized at 20 kHz using a ITC16 computer interface (Instrutech Corp., Long Island, NY, low-pass filtered at 3 kHz and stored on-line on the hard-drive of the computer. Electrodes were pulled on a PIP5 puller (HEKA, Germany) in two stages from borosilicate glass capillaries (PG52151, World Precision Instruments, Aston, UK) to a tip diameter giving a pipette resistance of 5 M Ω . For each cell, the membrane potential was clamped initially at -80 mV and the passive membrane components (membrane resistance and capacitance) were determined immediately after the establishment of the whole cell configuration. A protocol to assess the current/voltage (I/V) relationship was then initiated. For such experiments, a p/n protocol (8 negative prepulses a 1/10th of the pulse magnitude) was used to correct for the background leak and capacitive membrane currents.

Calcium Imaging

LNCaP cells were grown on glass coverslips to carry out calcium imaging experiments. Cytosolic calcium concentration was measured using Fura-2-loaded cells (18). LNCaP cells were loaded for 45 min at room temperature with 2 μ M Fura-2/AM prepared in Hank's balanced salt solution and subsequently washed three times with the same dye-free solution. The coverslip was then transferred onto a perfusion chamber on a Olympus IX70 microscope equipped for fluorescence. Fluorescence was alternatively excited at 340 and 380 nm with a monochromator (Polychrome IV, TILL Photonics GmbH, Planegg, Ger-

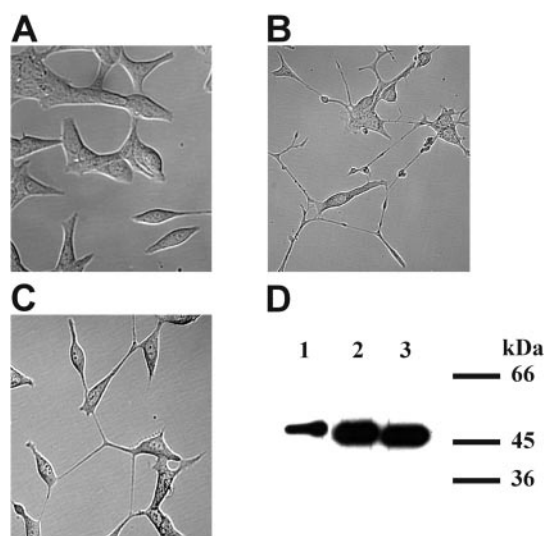


FIG. 1. Treatments for 3 days with Bt₂cAMP or IBMX induce neuroendocrine differentiation of LNCaP cells. A, untreated cells. B, cells treated with 1 mM Bt₂cAMP. C, cells treated with 100 μM IBMX. D, Western blot analysis of neuron-specific enolase expression. Lane 1, control cells. Lane 2, Bt₂cAMP. Lane 3, IBMX

many) and was captured after filtration through a long-pass filter (510 nm) by a MicroMax 5MHz CCD camera (Princeton Instruments, Evry, France). Acquisition and analysis was performed with the Metafluor 4.5 software (Universal Imaging Corp., West Chester, PA). The intracellular calcium concentration was derived from the ratio of the fluorescence intensities for each of the excitation wavelengths (F340/F380) and from the equation of Grynkiewicz *et al.* (18). All recordings were carried out at room temperature. The cells were continuously perfused with the Hank's balanced salt solution and chemicals were added via the perfusion system. The flow rate of the whole chamber perfusion system was set to 1 ml/min and the chamber volume was 500 μl.

Morphometric Analysis

Pictures of cultured LNCaP cells were recorded with a MicroMax 5 MHz CCD camera (Princeton Instruments, Evry, France). For each condition, at least 10 fields of cells were analyzed from two different batches of culture (total number of cells between 345 and 826). Images (1380 × 1030 pixels) were then analyzed and neurite processes were measured using an imaging software.

Chemicals

All chemicals were purchased from Sigma except for Fura-2 which was bought from Calbiochem (France Biochem, Meudon, France).

Statistical Analysis

Plots were produced using Origin 5.0 (Microcal Software, Inc., Northampton, MA). Results are expressed as mean ± S.E. Statistical analysis were performed using unpaired *t* tests or ANOVA tests followed by either Dunnett (for multiple control *versus* test comparisons) or Student-Newman-Keuls post-tests (for multiple comparisons).

RESULTS

Neuroendocrine Differentiation Induced by cAMP Permeant Analogs Is Associated with an Increased Inward Current—We first assessed by morphometric assays and Western blotting that culturing LNCaP cells for 3–5 days with cAMP permeant analogs (dibutyryl cAMP (Bt₂cAMP), 8-bromo-cAMP (8-Br-cAMP), 1 mM) or a phosphodiesterase inhibitor (isobutylmethylxanthine, IBMX, 100 μM) induced neuroendocrine differentiation. Treatment with Bt₂cAMP or IBMX (Fig. 1, A–C) or 8-Br-cAMP (not shown) led to neurite extension. In addition, treatments with Bt₂cAMP or IBMX enhanced the expression of a neuroendocrine marker, neuron-specific enolase (Fig. 1D). Morphological differentiation assessed by the presence of neurite extension was initiated as soon as 2 h after the onset of the treatment with Bt₂cAMP, 8-Br-cAMP, or IBMX.

Voltage-dependent calcium currents were then investigated

in non-treated (control) and treated LNCaP cells in conditions where voltage-dependent potassium channels were eliminated (see “Experimental Procedures”). Fig. 2A represents a typical experiment performed on a control cell. No significant voltage-dependent inward current was observed on this control cell. On the opposite, a cell treated with Bt₂cAMP for 3 days displayed an inward current activating at membrane potentials positive to –40 mV and peaking around –10 mV (Fig. 2B). The inward current reached its peak value 15 ms after the beginning of the voltage step to –10 mV and then exponentially decayed with a time constant of 20.3 ms (Fig. 2C). On average, the transient inward current activated and inactivated with exponential time constants of 11.6 ± 0.9 and 23.9 ± 1.5 ms, respectively.

After normalization of the peak inward current to the membrane capacitance (indicative of the cell surface area) for each cell, we observed that after 3–5 days of treatment, the average current density was significantly increased in cells treated with Bt₂cAMP at all membrane potentials between –40 and +20 mV (Fig. 2D, control cells: *n* = 96; 9 batches of cells, Bt₂cAMP-treated cells: *n* = 119; 11 batches of cells). The maximum current density was –0.81 ± 0.07 pA/pF at –10 mV for Bt₂cAMP-treated cells *versus* –0.35 ± 0.05 pA/pF for control cells, this corresponding to a 2.3-fold increase. The voltage-dependent transient current was only occasionally present in control cells (22 ± 6%), this proportion being enhanced (Fig. 2E) after treatment with Bt₂cAMP (62 ± 8%). Fig. 2F shows that the distribution of the current amplitude (at –10 mV) in control cells follows a normal curve but that there is a multi-peak distribution following treatment with Bt₂cAMP during 3–5 days with the emergence of a cell population with larger current densities (19% of treated cells with a current density larger than 1.5 pA/pF *versus* 3% for control cells).

The enhancement of this voltage-dependent transient inward current followed a slow kinetics. A 5-min application of Bt₂cAMP (1 mM) did not induce or increase such a current on control LNCaP cells (Fig. 2G, *n* = 9). Whereas a 1-day Bt₂cAMP treatment was ineffective, a 3-day treatment led to a significant and almost maximal increase in the transient current density (Fig. 2H). A 3-day treatment with another cAMP permeant analog, 8-Br-cAMP (1 mM), also raised the transient current density (–0.7 ± 0.08 pA/pF, *n* = 26, Fig. 2I). In addition, Bt₂cAMP action was potentiated by about 35% (Fig. 2J) by inhibiting the degradation of cAMP using IBMX (transient current density after Bt₂cAMP + IBMX (100 μM) = –1.09 ± 0.11 (*n* = 29)).

Biophysical and Pharmacological Characterization of the Inward Current Stimulated during Neuroendocrine Differentiation—We then investigated the ionic nature of this transient current observed in Bt₂cAMP-treated cells. As shown in Fig. 3, A and B, changing the external Na-containing solution to a Na-deprived solution (sodium being replaced by choline) did not significantly affect, whereas eliminating external calcium (calcium free solution and 0.1 mM EGTA) completely abrogated the transient inward current (*n* = 8). This shows that the ion channel evidenced in our studies belongs to the family of voltage-gated calcium channels which can be further distinguished by their kinetics and voltage dependence of activation, inactivation and deactivation in LVA and HVA calcium channels (19).

As shown above (Fig. 2), the inward current inactivated rapidly after the beginning of the depolarization. Since kinetics and voltage dependence may be indicative of the calcium channel nature, we have investigated its voltage-dependent inactivation (Fig. 3, C and D). This showed that the current during the test pulse followed a voltage-dependent inactivation. The inactivation began to occur for a membrane potential of –60

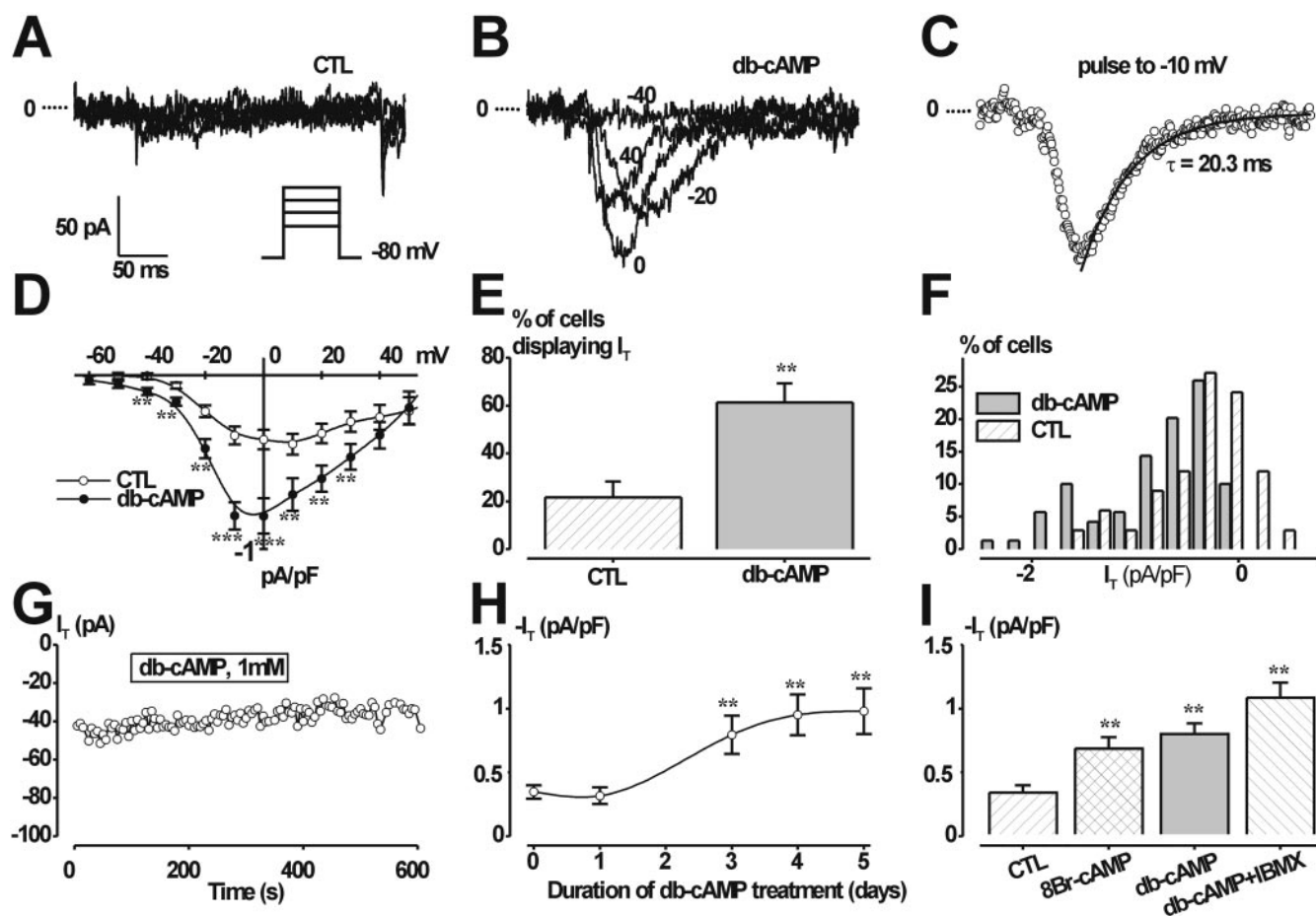


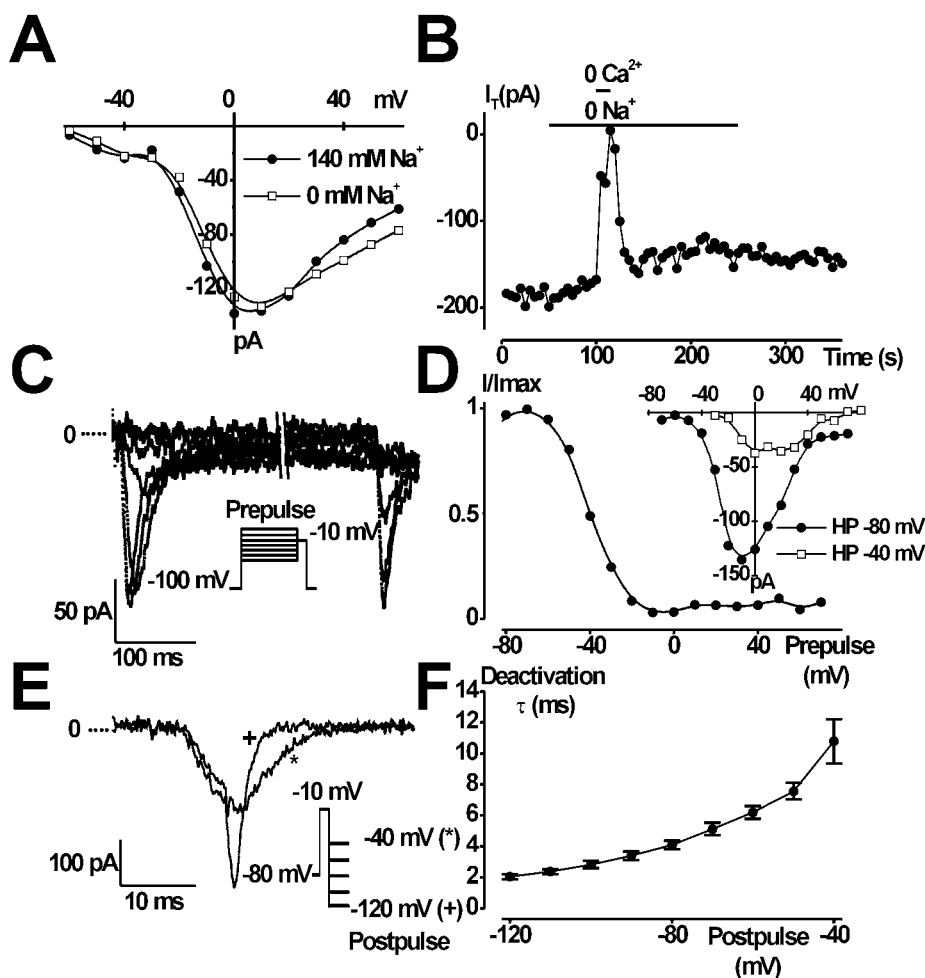
FIG. 2. Overexpression of a voltage-dependent inward current during neuroendocrine differentiation of LNCaP cells. *A–C*, examples of membrane currents in an untreated cell (*A*, CTL: control) and in a cell treated with Bt_2cAMP (*db-cAMP*) (*B–C*, 1 mM) for 3 days. Membrane potential was depolarized for 100 ms from -80 mV to different values shown next to the respective current recordings. The voltage pulse protocol is shown in *A* (inset). *C*, membrane current elicited by a depolarization from -80 to -10 mV in a Bt_2cAMP -treated cell (same as in *B*). For clarity, only one membrane current value (open circle) out of 10 was plotted. The current was fitted to an exponential function and displayed a time-dependent inactivation following a single exponential time constant (20.3 ms). *D*, average current/voltage (*I/V*) relationships for control (open circle) and Bt_2cAMP -treated cells (solid circles). *E*, proportion of cells displaying an inward current (I_T , T standing for transient) following an *I/V* curve similar to the one shown in *D*. *F*, membrane current density histogram showing that Bt_2cAMP treatments induced the emergence of a cell population with larger current densities. *G*, a 5-min bath application of 1 mM Bt_2cAMP did not alter the inward transient current observed in a control cell. *H*, whereas a 1-day treatment with Bt_2cAMP (1 mM) was ineffective, a 3–5-day treatment increased the transient current density. *I*, the transient current density was increased by a 3-day treatment with Bt_2cAMP (1 mM), 8-Br-cAMP (1 mM) or Bt_2cAMP and IBMX (100 μ M). **, $p < 0.01$; ***, $p < 0.001$. Comparisons were performed using an unpaired *t* test (panel *E*) or an ANOVA followed by a Dunnett post-test (panels *H* and *I*).

mV during the prepulse and was complete at -10 mV. Fig. 3*D* (inset) shows that the transient inward current was not completely abolished at -40 mV. To determine precisely the nature of the channel involved in the transient calcium current, we measured the deactivation kinetics of the calcium current. A characteristic feature of the T-type calcium channel is its slow deactivation: these channels deactivate with an exponential time constant of about 2 ms at -80 mV when compared with other voltage-dependent calcium channels (19, 20) which deactivate more than 10 times faster. The kinetics of deactivation during the tail current measured after a test pulse (Fig. 3*E*) was fitted to a single exponential and a time constant τ was computed and plotted as a function of the membrane potential during repolarization (Fig. 3*F*). As illustrated by the Fig. 3*F*, the time constant τ varied with the repolarization potential and was comprised between 2 ± 0.16 and 10.8 ± 1 ms for -120 and -40 mV, respectively.

The overall biophysical characteristics of the calcium current expressed in differentiated LNCaP cells suggest that this current belongs to the LVA-T type family of calcium currents. This was confirmed by an absence of action of HVA calcium channel

antagonists (nifedipine (0.5 μ M) for L-type, ω -conotoxin GVIA (50 nM) for N-type, ω -agatoxine (20 nM) for P/Q type calcium channels (not shown). We then assessed the sensitivities of the inward current to both nickel and cadmium since they vary according to the nature of the calcium channel, T-type calcium channels being more sensitive to nickel than to cadmium, on the contrary to HVA calcium channels (19, 21). Fig. 4 shows that $NiCl_2$ dose dependently inhibited the transient calcium current with an IC_{50} of 2.4 ± 0.4 μ M and a maximal inhibition of $90.8 \pm 3.4\%$, whereas $CdCl_2$ dose dependently abolished the calcium current with an IC_{50} of 58.8 ± 8.9 μ M. We then used mibefradil (Ro 40-5967), the most selective antagonist to voltage-dependent T-type calcium channels (22, 23). As shown on Fig. 4, mibefradil (20 μ M) induced a reversible and dose-dependent reduction of the transient calcium current at all membrane potentials. At -10 mV, mibefradil reduced the transient calcium current by $74 \pm 4\%$ ($n = 8$). The IC_{50} was found to be around 5 μ M. Our experiments demonstrate that 5 μ M flunarizine (a piperazine derivative previously shown to inhibit T-type calcium channels (24)) reversibly decreased by $62 \pm 3\%$ the transient calcium current ($n = 3$).

FIG. 3. Biophysical properties of the transient inward current (I_T) expressed in differentiated LNCaP cells. *A*, *I/V* curves in the presence and absence of sodium in the bath solution. *B*, changing the external sodium for choline did not inhibit whereas removing calcium (using a calcium-free solution and 0.1 mM EGTA) abolished the transient current. Voltage protocols for *A* and *B* were the same as in Fig. 2. *C*, the transient inward current displayed a voltage-dependent inactivation. Cells were submitted for 1 s to a prepulse from -100 mV to different membrane potential values and a test pulse was applied for 100 ms at -10 mV (protocol shown in *inset*). Traces were interrupted for clarity. *D*, plot of the membrane current during the test pulse as a function of the prepulse potential. The transient current was half-inactivated at -40 mV. *Inset*, *I/V* curves obtained for a holding potential of -40 mV or -80 mV. *E*, deactivation tail currents measured after a 10-ms prepulse for a repolarization potential (postpulse) of -40 mV (*) or -120 mV (+) (protocol shown in *inset*). *F*, plot of the deactivation time constant, τ , as a function of the repolarization potential.



The above results suggest that treatments with cAMP analogs increase the number of calcium channels in the plasma membrane. To study whether the T-type calcium current could be regulated in another way than an overexpression, we checked whether cAMP analogs induced a change in the characteristics of the T-type calcium current. Membrane currents obtained after a 3–5-day treatment with Bt_2cAMP , or Bt_2cAMP + IBMX, in addition to membrane currents recorded in control cells, were normalized to the maximum current. The treatments induced no shift in the voltage sensitivity of the calcium current as evidenced by the similarity of all the normalized *I/V* curves (Fig. 5*A*). A similar *I/V* curve was obtained for 8-Br-cAMP-treated cells (not shown). Activation and inactivation curves (Fig. 5, *B* and *C*) were computed for control cells ($n = 5$), Bt_2cAMP ($n = 6$, not shown), and Bt_2cAMP + IBMX-treated cells ($n = 10$). Data from each condition were fitted to a Boltzmann equation. These curves showed no significant differences in the mid-point of voltage dependence ($V_{0.5}$) nor in the slope factor (k). In both untreated and treated cells, the $V_{0.5}$ were close to -17 mV and -39 mV and the slope factors were close to 7 mV and -7 mV, for activation and inactivation, respectively. In addition, the kinetics of time-dependent activation and inactivation were not altered. Time constants of activation were 8.7 ± 0.8 versus 11.6 ± 0.9 ms and time constants of inactivation were 24.8 ± 2.4 versus 23.9 ± 1.5 ms, for control and treated cells, respectively.

Overexpression of an α_{1H} T-type Calcium Channel after Treatment by cAMP Permeant Analogs—To determine which subtypes of calcium channels are expressed in LNCaP cells, we elaborated one-step RT-PCR, using seven distinct sets of primers (Table I) designed according to the human sequence of

specific regions (corresponding to the second large intracellular loop linking domains II and III, L_{II-III}) of the corresponding α_1 channel subunits. The three T-type channel isoforms (α_{1G} , α_{1H} , and α_{1I}) and the four L-type channel isoforms (α_{1C} , α_{1D} , α_{1S} , and α_{1F}) were tested. Analysis of RT-PCR products revealed the presence of one single fragment corresponding to the α_{1H} amplicon in control cells (Fig. 6*A*) while other channel isoforms were not detected. In LNCaP cells treated with Bt_2cAMP (1 mM, 1 or 3 days) and with IBMX (100 μ M) + Bt_2cAMP (3 days), only the α_{1H} isoform was detected, as in control cells (figure not shown). Similarly, mRNA coding for the GAPDH, a housekeeping gene used for normalizing the initial amount of RNA, was reverse transcribed and amplified with specific primers in the same experiment.

To compare the mRNA coding for α_{1H} in control and treated cells, we used a real-time RT-PCR approach that combines the high sensitivity of the PCR technique with the accuracy supplied by a continuous monitoring of a fluorescent signal proportional to the accumulated PCR product, as previously described in detail by Lesouhaitier *et al.* (25). This analysis has been performed on a LightCycler system (Roche Molecular Diagnostics) with online detection of the fluorescent dye SYBR Green I, that is excitable only when inserted in double stranded DNA. The variation of mRNA coding for α_{1H} channel was studied in cells submitted to various treatments known to increase cytosolic cAMP concentration in prostate LNCaP cells, Bt_2cAMP (1 mM), 8-Br-cAMP (1 mM), or a combination of both Bt_2cAMP and IBMX (100 μ M). Treatments were applied for 1 or 3 days. To minimize errors due to variations occurring during RNA extraction and quantification, the results were normal-

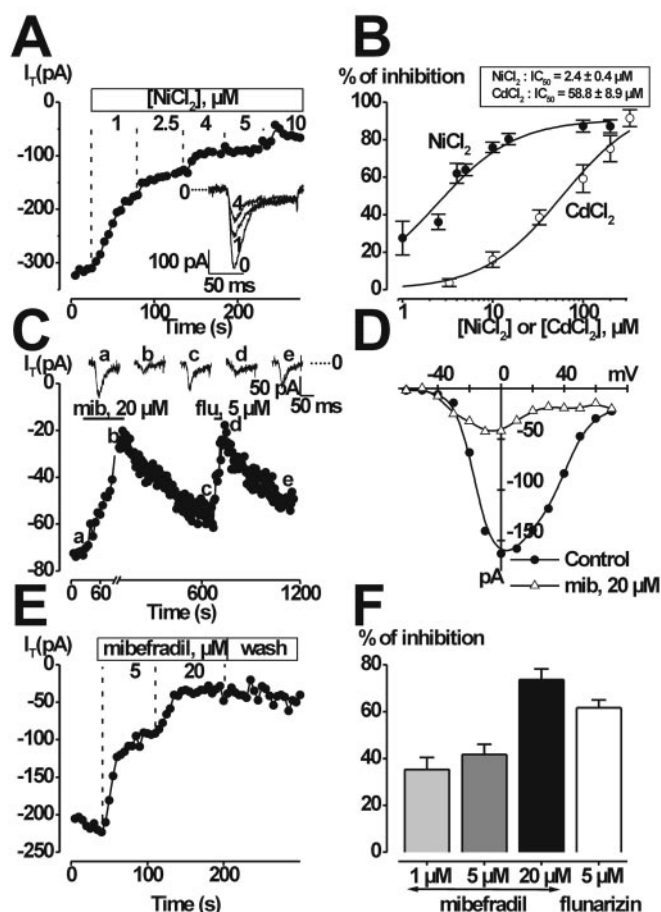


FIG. 4. Pharmacological properties of the transient inward current (I_T) expressed in differentiated LNCaP cells. A, increasing concentrations of NiCl_2 dose dependently inhibited I_T in a differentiated LNCaP cell. *Inset*, membrane currents for 3 concentrations of NiCl_2 (0, 1, and 4 μM). B, plot of the % of I_T inhibition as a function of NiCl_2 and CdCl_2 concentrations ($n = 3$ to 8 for each concentration). The curves were fitted to logistic dose-response functions, giving an IC_{50} of 2.4 μM for NiCl_2 inhibition and 58.8 μM for CdCl_2 inhibition. C, kinetics of mibefradil (*mib*)- and flunarizin (*flu*)-induced I_T inhibition. On the top of the panel is shown the membrane current at different times of the experiment (a–e). D, I/V curves in the absence (solid circles) and presence (open triangles) of 20 μM mibefradil. E, increasing concentrations of mibefradil dose-dependently inhibited I_T . F, bar chart summary of mibefradil- and flunarizin-induced I_T inhibitions (mibefradil 1 μM : $n = 3$; 5 μM : $n = 16$; 20 μM : $n = 8$; flunarizin: $n = 3$).

ized to the amount of mRNA coding in the same sample for GAPDH, the expression of which was unaffected by treatments. Analysis of GAPDH was also useful as quality control for the RNA extraction procedure. All the treatments led to an enhanced expression of the $\alpha_{1\text{H}}$ messenger after 3 days. A treatment for 3 days with Bt_2cAMP increased by 2.6-fold the ratio $\alpha_{1\text{H}}/\text{GAPDH}$. The most efficient treatment was the combination of both Bt_2cAMP and IBMX which increased by 5-fold the $\alpha_{1\text{H}}$ mRNA expression. This increased expression of $\alpha_{1\text{H}}$ mRNA was time-dependent since no significant increase could be obtained after 1 day of treatment (Fig. 6B).

The $\alpha_{1\text{H}}$ T-type Calcium Channel Is Involved in a Window Calcium Current Promoting Calcium Entry at Resting Potentials—We then studied the involvement of the $\alpha_{1\text{H}}$ calcium channel in calcium homeostasis of LNCaP cells. T-type calcium channels generate transient inward currents which rapidly inactivate (exponential time constant 20 ms in our experiments). It was previously shown in other cell models that there may be a range of membrane potentials at which T-type calcium channels are activated, even partially, and at which in-

activation is not complete (26). There should thus exist a window of potential allowing a sustained calcium current. From the inactivation curves and the current voltage relationship (Fig. 3), we computed the relative activation and inactivation conductance and fitted them to a Boltzmann equation. The window current was calculated by multiplying the normalized inactivation curve (Fig. 7A) by the non-normalized activation curve. As shown in Fig. 7B, the maximum predicted window current is significant from -40 to -20 mV with a peak at -30 mV. Therefore, there should be a sustained calcium entry at these membrane potentials occurring through T-type calcium channels. We measured the resting membrane potential of LNCaP cells and found it to be very close to -30 mV. Control cells had a resting membrane potential of -29.9 ± 1.4 mV ($n = 10$), whereas Bt_2cAMP -treated cells and $\text{Bt}_2\text{cAMP} + \text{IBMX}$ -treated cells had a resting membrane potential of -35.3 ± 3.8 mV ($n = 10$) and -34 ± 4 mV ($n = 5$), respectively. These data show that T-type calcium channels may be open at resting potential in LNCaP cells. We carried out experiments to assess whether this putative window calcium current could lead to a basal sustained calcium entry and thus to higher cytosolic calcium levels in differentiated cells. Cells were loaded with 2 μM Fura-2/AM to measure cytosolic free calcium concentration. As shown in Fig. 8A, the basal calcium concentration of LNCaP cells was altered by a 3-day pretreatment with Bt_2cAMP , 8-Br-cAMP (Br-cAMP), or IBMX. In all cases, the average basal calcium concentration ($n = 100$ to 200 cells) was significantly higher in treated cells than in non-treated cells (46.2 ± 0.9 , 61.4 ± 2.1 , 55.7 ± 1.6 , and 61.8 ± 1.8 nM for CTL, Bt_2cAMP , 8-Br-cAMP, and IBMX-treated cells, respectively). Differences were small (10–15 nM) but were significant and reproduced with 5 different batches of cells. We investigated the ability of NiCl_2 to decrease the basal-free calcium concentration in both control and treated cells. Mibefradil was not used in these experiments since it appeared to have side effects and in addition to block calcium entry, was also able to produce a calcium rise in some cells (not shown). Fig. 8, B and C, show the relative variation of $[\text{Ca}^{2+}]_i$ after the application of different concentrations of NiCl_2 . As shown in Fig. 8B, NiCl_2 (20 μM) was much more effective to reduce $[\text{Ca}^{2+}]_i$ in cells treated 3–4 days with Bt_2cAMP or IBMX ($\Delta[\text{Ca}^{2+}]_i = -28.8 \pm 2.9$ and -21.6 ± 2.5 nM, respectively) than in control cells ($\Delta[\text{Ca}^{2+}]_i = -4 \pm 0.9$ nM). Cells treated with 8-Br-cAMP (1 mM) were also more sensitive to NiCl_2 than control cells (maximal $\Delta[\text{Ca}^{2+}]_i = -12.7 \pm 2.3$ nM). As shown in Fig. 8C, the reduction of $[\text{Ca}^{2+}]_i$ by NiCl_2 was dose-dependent with a concentration of 5 μM being only half effective as 20 μM in decreasing the basal cytosolic calcium concentration in Bt_2cAMP -treated cells. In addition, we observed that the basal calcium entry was inhibited by potassium depolarization (KCl, 100 mM) and that an application of NiCl_2 (20 μM) during depolarization, which should lead to full inactivation of T-type calcium channels, was not anymore able to reduce the cytosolic calcium concentration (not shown).

Physiological Implication of Voltage-dependent Calcium Channels—To identify the putative involvement of T-type calcium channels in prostate cell physiology, we first studied the influence, on voltage-dependent calcium currents, of steroid reduction, previously reported to induce neuroendocrine differentiation (10, 11). Indeed, LNCaP cells cultured in steroid-reduced conditions displayed a morphological differentiation as shown on Fig. 9 by the extension of neurites. In steroid-reduced conditions, most LNCaP cells ($59.6 \pm 7.7\%$, $n = 44$) displayed a voltage-dependent inward current similar to the Bt_2cAMP -induced current. Steroid reduction induced both an increase in the fraction of cells expressing the voltage-dependent current and the average current density (0.89 ± 0.1 pA/pF). However,

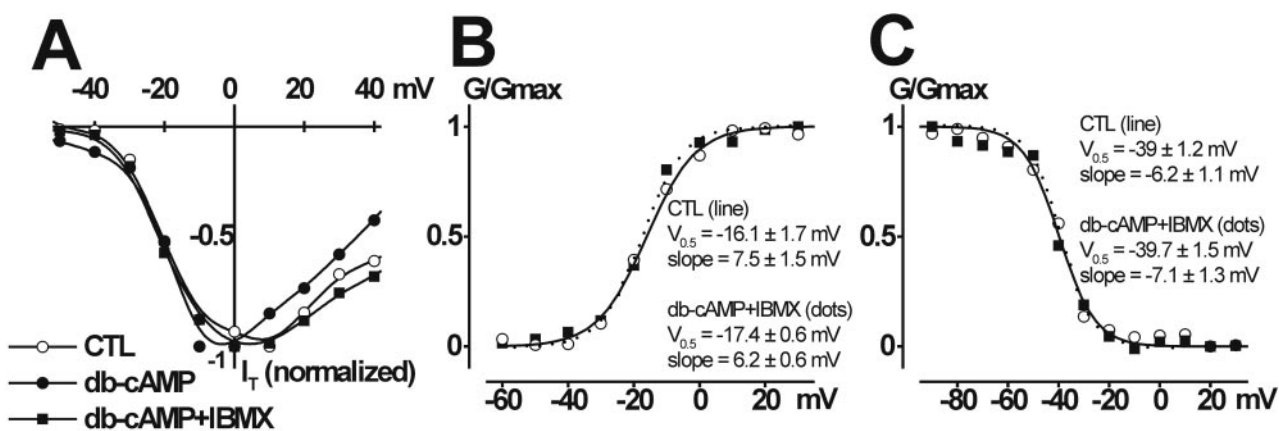


FIG. 5. A 3–5 days treatment inducing neuroendocrine differentiation does not alter I_T properties. A, normalized I/V curves for control cells (CTL), Bt_2cAMP (*db-cAMP*)-treated cells and Bt_2cAMP + IBMX-treated cells. For each curve, the current for each membrane potential was divided by the absolute value of the maximal current. B, activation; and C, inactivation curves for control cells and Bt_2cAMP + IBMX-treated cells (reversal potential = 80 mV).

TABLE I
Sequence of selected oligonucleotides used as RT-PCR primers

Target	Forward	Reverse	Product size
			bp
α_{1G}	5'-GAGCCCGATTCTTCTCACC	5'-CGGTGACTTCATCTCGTGG	256
α_{1H}	5'-TCGAGGAGGACTTCCACAAG	5'-TGCATCCAGGAATGGTGAG	177
α_{1I}	5'-AGGATGAGCTATGACCAGCG	5'-CAGAGAGCAGGGACTCATGC	151
α_{1C}	5'-CAAGAGTTGGTGGAGAAGCC	5'-TGAAGCTCAGAGAGTGTGTC	236
α_{1D}	5'-AGCCAACAGTGACAACAAGG	5'-TTCAACTCCGAGATCCTTCG	169
α_{1S}	5'-GATGACGAGGAAGATGAGCC	5'-AAGATGAAGAAGGAGCTGGC	117
α_{1F}	5'-GAGCAGACATGGAGGAGGAG	5'-TGGCTGAGGCAGAAGAAGG	154
GAPDH	5'-GAAGGTGAAGGTCGGAGTC	5'-GAAGATGGTATGGGATTC	228

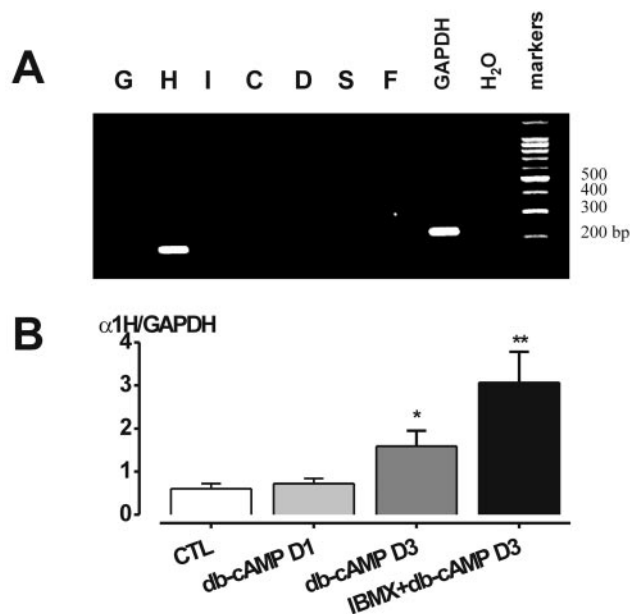


FIG. 6. T-type α_{1H} calcium channel mRNA is overexpressed in LNCaP cells during neuroendocrine differentiation. A, RT-PCR analysis reveals the presence of α_{1H} mRNA in control cells while other channel isoforms were not detected. mRNA coding for the GAPDH was present and amplified with specific primers in the same experiment. B, real-time SYBR Green RT-PCR reveals that all the treatments inducing neuroendocrine differentiation led to an enhanced expression of the α_{1H} messenger after 3 days (D1 and D3, 1 or 3 days treatment, respectively). Results were normalized to the amount of mRNA coding in the same sample for GAPDH, a housekeeping gene, the expression of which was unaffected by treatments. *db-cAMP*, Bt_2cAMP .

the kinetics of both steroid-induced differentiation and the voltage-dependent calcium current induction were much slower than with cAMP permeant analog treatments since

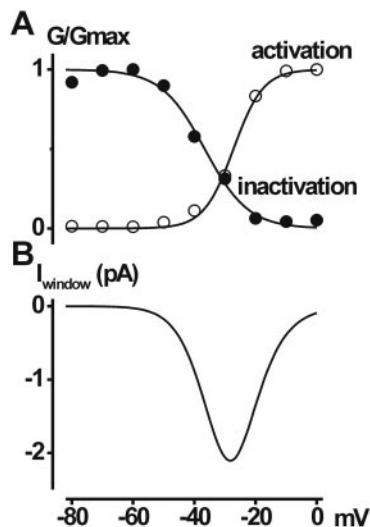


FIG. 7. T-type calcium channels may carry a window calcium current in differentiated LNCaP cells. A, normalized activation (open circles) and inactivation (solid circles) conductance curves (holding potential between steps was -100 mV). B, predicted window calcium current computed by multiplying the normalized inactivation conductance (A) by the activation conductance (not normalized).

neurite extensions were evident after more than 3 days in the absence of steroids and since the calcium current was recorded only after a treatment period of 1 week (only $16.3 \pm 3.8\%$ of cells expressed the T-type calcium current after 3 days of treatment, $n = 18$, Fig. 9). As shown on Fig. 9A (inset), this calcium current displayed a slow deactivation.

We then investigated the implication of voltage-dependent calcium channels in neurite elongation. Neurite lengths were measured from digital pictures of LNCaP cells (see Fig. 10A) cultured for 1 or 5 days in either control or stimulated (1 mM

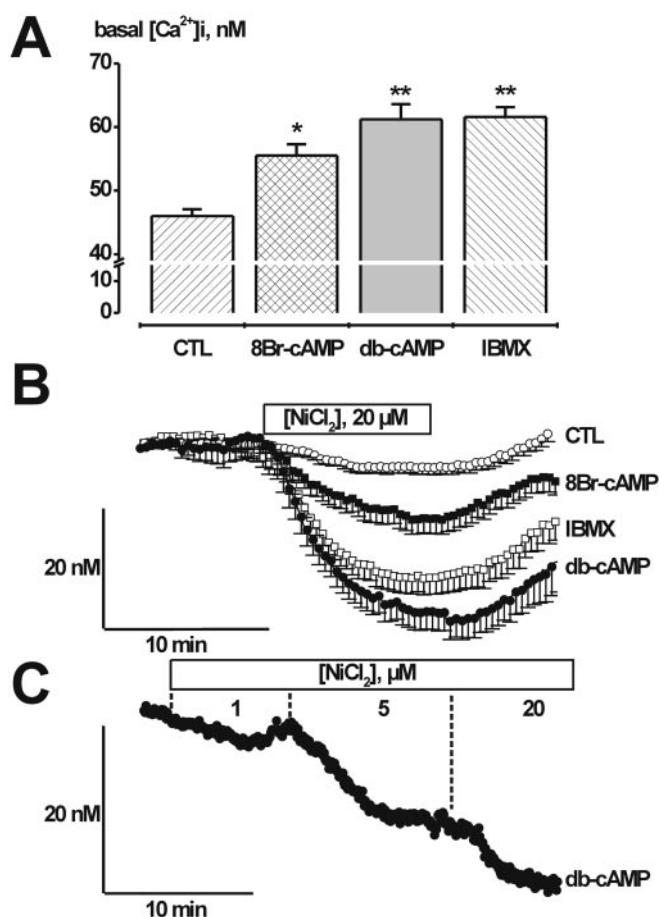


FIG. 8. Calcium homeostasis is altered during neuroendocrine differentiation induced by increasing cytosolic cAMP concentrations. *A*, resting calcium concentration ($[Ca^{2+}]_i$) in LNCaP cells after 3 days of treatment (1 mM 8-Br-cAMP, 1 mM Bt_2cAMP (*db-cAMP*), or 100 μM IBMX). *B* and *C*, dynamic $[Ca^{2+}]_i$ recording in Fura 2-loaded LNCaP cells. *B*, a bath application of 20 μM $NiCl_2$ decreases cytosolic resting calcium levels in LNCaP cells, this decrease being more pronounced in differentiated cells. Each trace represents the mean \pm S.E. of 100–200 cells for each condition. All the traces were set to the same initial value at the beginning of the plot to compare the variation of $[Ca^{2+}]_i$. *C*, progressively increasing the bath concentration of $NiCl_2$ from 1 to 20 μM induces a staircase decrease in $[Ca^{2+}]_i$ in differentiated cells (the plot represents the mean of 150 cells). Comparisons were performed using an ANOVA followed by a Dunnett post-test.

Bt_2cAMP and 100 μM IBMX) conditions in the absence or presence of $NiCl_2$ (20 μM , 100 μM). cAMP-induced neurite lengthening was not statistically affected by the presence of 20–100 μM $NiCl_2$ if the treatment lasted only 1 day (not shown) but was reduced by 30–37% after a 5-day treatment (Fig. 10B). However, the increased expression of NSE induced by a treatment with both Bt_2cAMP and IBMX for 5 days was not modified by the presence of $NiCl_2$ (20 μM , not shown).

DISCUSSION

Neuroendocrine differentiation is a common feature of human prostate carcinoma (2, 3) and is considered to be associated with poor prognosis and reduced long-term survival (4). However, the molecular mechanisms linked to neuroendocrine differentiation development in the prostate epithelium are not fully understood. Therefore, their description are particularly relevant for the future development of therapeutical targets. To this end, different prostatic cell models have been developed, the most widely used being LNCaP prostate cells (5–9) expressing specific markers for neuroendocrine cells like NSE following treatment with cAMP permeant analogs (5, 8, 9). Neuroen-

docrine cells are generally characterized by the presence of voltage-gated calcium channels. We therefore carried out a study of the expression of such channels in LNCaP cells and followed their evolution during neuroendocrine differentiation. We report here for the first time the evidence of a basal expression of voltage-sensitive calcium channels in prostate cancer cells. Furthermore, and more importantly, we have demonstrated an up-regulation of voltage-gated calcium channels in prostate cancer cells during a treatment inducing a neuroendocrine differentiation as evidenced by a neurite extension and the overexpression of neuron-specific enolase.

The voltage-dependent current recorded in our study inactivates with time and potential and slowly deactivates. These properties are characteristic of T-type calcium currents since high-voltage activated L-, N-, P/Q-, and R-type calcium currents deactivate more rapidly (in less than 200 μs (19, 20)). The voltage-dependent calcium current we observed is certainly carried by a single type of voltage-dependent calcium channel expressed in LNCaP cells since we never observed a tail current deactivating with two exponential time constants. Furthermore, RT-PCR experiments showed the expression of only one subtype belonging to the α_1 subunit family which constitutes the pore subunit. To date, 10 different α_1 subunits have been cloned, among which three (α_{1G} , α_{1H} , and α_{1I}) have the biophysical and pharmacological properties of the native T-type calcium channels when overexpressed in *Xenopus* oocytes or HEK-293 cells (27–30). Our results indicate that prostate cancer cells only express the α_{1H} subunit. This is in good agreement with studies showing that the α_{1H} subunit is mostly distributed in peripheral tissues (28), on the contrary to α_{1G} and α_{1I} subunits expressed in the brain (29, 30). As recently shown (21), the α_{1H} subunit is highly sensitive to $NiCl_2$ (IC_{50} around 5 μM) and this sensitivity provides an assay for the expression of α_{1H} subunits (21, 29). Indeed, we observed that T-type calcium currents in LNCaP cells have a greater sensitivity to $NiCl_2$ ($IC_{50} = 2.5 \mu M$) over $CdCl_2$ ($IC_{50} = 60 \mu M$). Furthermore, in our study, the calcium current was inhibited by mibefradil, the best T-type calcium channel antagonist to date (22, 23, 31).

Our results clearly show that an α_{1H} T-type calcium channel is overexpressed during neuroendocrine differentiation of LNCaP cells. This was demonstrated by an increase in the average membrane current density paralleled by the overexpression of mRNA coding for the α_{1H} calcium channel isoform. The increase in membrane current was most unlikely due to a protein kinase A-dependent serine-threonine phosphorylation of the channels since changes in the calcium current density were not accompanied by any changes in the current characteristics, *i.e.* time and voltage-dependent activation and inactivation and since short-term applications of Bt_2cAMP were unable to increase the membrane current.

As previously demonstrated (10, 11), we confirm that steroid removal from the culture medium led to a morphological neuroendocrine differentiation with the appearance of neurite extensions after 3 days of culture, a delay much longer than with cAMP permeant analogs. This implies that neuroendocrine differentiation probably occurs through distinct intracellular pathways, as previously hypothesized (11), even if there are few evidences that depletion in androgens can increase intracellular cAMP (32) in prostate LNCaP cells. In addition, androgen removal increased the proportion of cells expressing the T-type calcium current and the overall calcium current density.

Recent studies have demonstrated that the α_{1H} subunit is involved in differentiation of myoblasts in myotubes (33) and that the α_{1G} subunit is differentially expressed during development (30). It seems unlikely that α_{1H} calcium channels are

FIG. 9. Steroid reduction promotes the overexpression of a T-type calcium current. **A**, examples of membrane currents in a LNCaP cell treated with steroid-reduced medium for 7 days. Membrane potential was depolarized for 100 ms from -80 mV to different values shown next to the respective current recordings (protocol shown in Fig. 2A, *inset*). *Inset*, deactivation tail currents measured after a 10-ms prepulse for a repolarization potential (postpulse) of -40 mV (*) or -100 mV (+) (protocol shown in Fig. 3E, *inset*). **B**, average I/V relationship for LNCaP cells cultured in steroid-reduced medium. **C**, proportion of cells displaying an inward current following an I/V curve similar to the one shown in **B** after 3 days ($-ST$ D3) and 7 days ($-ST$ D7) of treatment. Comparisons were performed using an ANOVA followed by a Dunnett post-test. **D**, pictures of LNCaP cells after 2 (*left panel*), 4 (*middle panel*), or 8 (*right panel*) days of treatment.

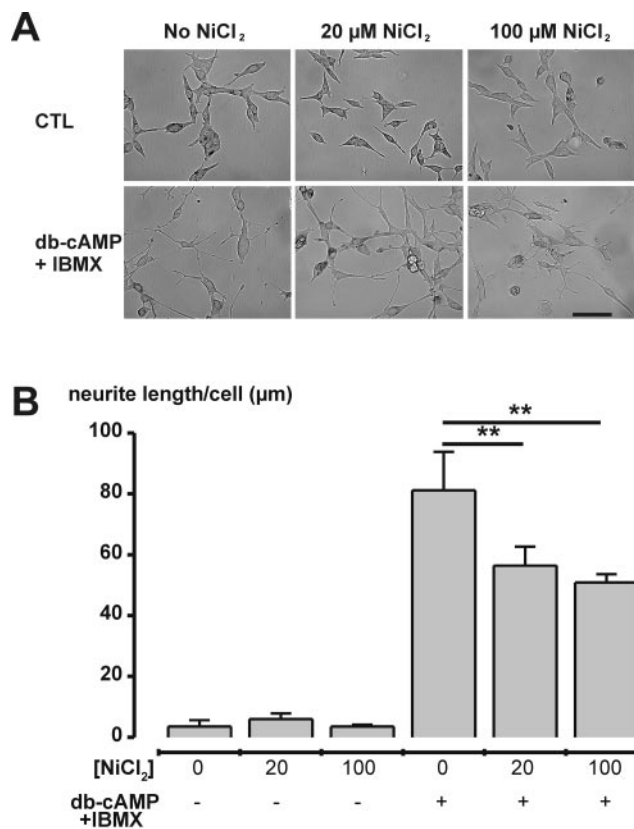
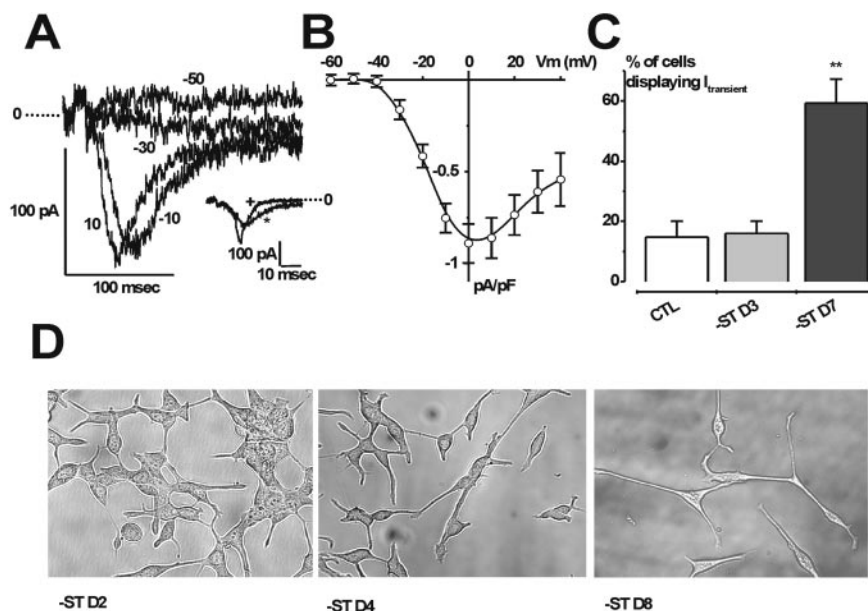


FIG. 10. T-type calcium channel inhibition reduces the neurite elongation triggered by cAMP permeant analogs. **A**, pictures of LNCaP cells without (*top panels*) or with 1 mM Bt₂cAMP (*db-cAMP*) and 100 μ M IBMX (*bottom panels*). The action of different concentrations of NiCl₂ (20 μ M, *middle panels*, and 100 μ M, *right panels*) was compared with the control situation (*left panels*). Scale bar, 50 μ m. **B**, bar chart summary of neurite lengths. Comparisons were performed using an ANOVA followed by a Student-Newman-Keuls post-test.

involved in triggering the neuroendocrine differentiation process itself since the morphological differentiation, induced by different stimuli, always preceded the overexpression of voltage-dependent calcium channels. Indeed, we have shown in this study that blocking T-type calcium currents with low concentrations of NiCl₂ (20–100 μ M) did not impede the extension of

neuritic processes triggered by cAMP permeant analogs. However, T-type calcium channels may have a potential role in maintaining neurite growth since long-term treatments (5 days) with NiCl₂ decreased cAMP-induced neurite lengthening by 30%. Further studies, using antisense and transfection strategies, will be necessary to delineate the involvement of α_{1H} calcium channels in prostate cancer cell physiopathology. Neuroendocrine differentiation is also associated with synchronization in phase G₁ of the cell cycle, cell growth arrest, and increased neuropeptide and prostate-specific antigen secretion in LNCaP cells (5, 8). Therefore, it will be of particular interest to assess α_{1H} calcium channels' role in cell growth and secretion. Indeed, T-type calcium channels have been suspected to be critical for cell cycle progression (34, 35) and were reported to be overexpressed in proliferating cells (36, 37). However, since transfection with different α_1 subunits corresponding to the LVA channel (G and H) does not modulate the proliferation HEK-293 cells, the evidence for a role of T-type calcium channels in cell proliferation are still very weak and remain debatable (38) and has to be determined in prostate cells. If this is the case, our data, when compared with the literature, would tend to attribute an inhibitory role for LVA calcium channels in cell growth.

We have shown that the T-type calcium channel continuous opening at resting membrane potential allows calcium entry, via a so-called calcium window current. We thus demonstrate that this α_{1H} calcium channel is involved in calcium homeostasis and that cytosolic calcium concentrations are modified during neuroendocrine differentiation, due to the overexpression of α_{1H} calcium channels, induced by permeant analogs of cAMP or IBMX. Such window currents occurring through T-type calcium channels have been reported in other cells (26, 29, 38). This slight increase in cytosolic calcium concentration may serve in facilitating neurite growth, as proposed in nerve cells (15). Furthermore, it is now well established that calcium homeostasis mechanisms are involved in the control of cell death (39). In prostate cancer cells, we have previously shown that altering intracellular calcium concentration may lead to apoptosis (40). It is therefore possible that calcium entry through α_{1H} calcium channels may be implicated in prostate cell death as it was described for T-type calcium channels in cytokine-induced cell death of pancreatic β cells (41) and in neuronal cells expressing expanded androgen receptors (42).

The role of T-type calcium channels may also be of great

importance in the control neuropeptide secretion by neuroendocrine prostate cells. Indeed, it was shown that secretion of mitogenic peptides by LNCaP cells is enhanced during neuroendocrine differentiation (5). Furthermore, it is known that calcium is the main ion involved in the control of exocytosis in many cell models and a fundamental role has been shown for L-type and N- and P/Q-type calcium channels in neuroendocrine cells (43). Few studies have demonstrated a direct role of T-type calcium channels in exocytosis (44). Since neuroendocrine differentiation of prostate cancer cells is associated with an increase in secretory granule number in the cytoplasm (8), an increase in serotonin immunofluorescence, in secretion of neurotensin and PTH-related peptides (5), it is conceivable that overexpression of α_{1H} T-type calcium channels would participate in triggering secretion in these cells. In relation to the role of α_{1H} T-type calcium channels in secretion, we cannot exclude that the reduction of neurite lengthening by NiCl_2 we have observed in our study may be due to the inhibition of secretion of paracrine factors having a growth/neurotrophic activity.

In summary, this study demonstrates for the first time the overexpression of voltage-gated T-type calcium channels in prostate cancer cells during neuroendocrine differentiation. Since neuroendocrine differentiation is a common feature of prostate cancer, the functional expression of these calcium channels could have fundamental consequences in understanding the etiology of prostate cancer. Future studies performed on prostate tissue obtained from surgery will be necessary to assess the expression of these channels, and particularly in the late stages of the disease when neuroendocrine differentiation develops.

Acknowledgments—We are particularly grateful to A. Chiappe for excellent technical assistance. We thank Drs. E.-M. Gutknecht and P. Weber for providing us with mibefradil (F. Hoffmann-La Roche, Basel, Switzerland).

REFERENCES

- Bonkhoff, H. (1998) *Prostate Suppl.* **8**, 18–22
- Abrahamsson, P. A. (1999) *Prostate* **39**, 135–148
- di Sant'Agnese, P. A. (1992) *Cancer* **70**, 254–268
- Cohen, R. J., Gleason, G., Haffjee, Z., and Afrika, D. (1990) *Br. J. Urol.* **66**, 405–410
- Cox, M. E., Deeble, P. D., Lakhani, S., and Parsons, S. J. (1999) *Cancer Res.* **59**, 3821–3830
- Qiu, Y., Robinson, D., Pretlow, T. G., and Kung, H. J. (1998) *Proc. Natl. Acad. Sci. U. S. A.* **95**, 3644–3649
- Mori, S., Murakami-Mori, K., and Bonavida, B. (1999) *Biochem. Biophys. Res. Commun.* **257**, 609–614
- Bang, Y. J., Pirnia, F., Fang, W. G., Kang, W. K., Sartor, O., Whitesell, L., Ha, M. J., Tsokos, M., Sheahan, M. D., Nguyen, P., Niklinski, W. T., Myers, C. E., and Trepel, J. B. (1994) *Proc. Natl. Acad. Sci. U. S. A.* **91**, 5330–5334
- Cox, M. E., Deeble, P. D., Bissonette, E. A., and Parsons, S. J. (2000) *J. Biol. Chem.* **275**, 13812–13818
- Zi, X., and Agarwal, R. (1999) *Proc. Natl. Acad. Sci. U. S. A.* **96**, 7490–7495
- Zelivianski, S., Verni, M., Moore, C., Kondrikov, D., Taylor, R., and Lin, M. F. (2001) *Biochim. Biophys. Acta* **1539**, 28–43
- Garber, S. S., Hoshi, T., and Aldrich, R. W. (1989) *J. Neurosci.* **9**, 3976–3987
- Solem, M., McMahon, T., and Messing, R. O. (1995) *J. Neurosci.* **15**, 5966–5975
- Sherwood, N. T., Lesser, S. S., and Lo, D. C. (1997) *Proc. Natl. Acad. Sci. U. S. A.* **94**, 5917–5922
- Spitzer, N. C., Lautermilch, N. J., Smith, R. D., and Gomez, T. M. (2000) *Bioessays* **22**, 811–817
- Shitaka, Y., Matsuki, N., Saito, H., and Katsuki, H. (1996) *J. Neurosci.* **16**, 6476–6489
- Hamill, O. P., Marty, A., Neher, E., Sakmann, B., and Sigworth, F. J. (1981) *Pflugers Arch.* **391**, 85–100
- Grynkiewicz, G., Poenie, M., and Tsien, R. Y. (1985) *J. Biol. Chem.* **260**, 3440–3450
- Randall, A. D. (1998) *J. Membr. Biol.* **161**, 207–213
- Matteson, D. R., and Armstrong, C. M. (1986) *J. Gen. Physiol.* **87**, 161–182
- Lee, J. H., Gomora, J. C., Cribbs, L. L., and Perez-Reyes, E. (1999) *Biophys. J.* **77**, 3034–3042
- Rossier, M. F., Ertel, E. A., Vallotton, M. B., and Capponi, A. M. (1998) *J. Pharmacol. Exp. Ther.* **287**, 824–831
- McDonough, S. I., and Bean, B. P. (1998) *Mol. Pharmacol.* **54**, 1080–1087
- Dzhura, I., Kostyuk, P., Lyubanova, O., Naidenov, V., and Shuba, Y. (1994) *Neuroreport* **5**, 1960–1962
- Lesouhaitier, O., Chiappe, A., and Rossier, M. F. (2001) *Endocrinology* **142**, 4320–4330
- Rossier, M. F., Aptel, H. B., Python, C. P., Burnay, M. M., Vallotton, M. B., and Capponi, A. M. (1995) *J. Biol. Chem.* **270**, 15137–15142
- Perez-Reyes, E., Cribbs, L. L., Daud, A., Lacerda, A. E., Barclay, J., Williamson, M. P., Fox, M., Rees, M., and Lee, J. H. (1998) *Nature* **391**, 896–900
- Cribbs, L. L., Lee, J. H., Yang, J., Satin, J., Zhang, Y., Daud, A., Barclay, J., Williamson, M. P., Fox, M., Rees, M., and Perez-Reyes, E. (1998) *Circ. Res.* **83**, 103–109
- Lee, J. H., Daud, A. N., Cribbs, L. L., Lacerda, A. E., Pereverzev, A., Klockner, U., Schneider, T., and Perez-Reyes, E. (1999) *J. Neurosci.* **19**, 1912–1921
- Monteil, A., Chemin, J., Bourinet, E., Mennessier, G., Lory, P., and Nargeot, J. (2000) *J. Biol. Chem.* **275**, 6090–6100
- Martin, R. L., Lee, J. H., Cribbs, L. L., Perez-Reyes, E., and Hanck, D. A. (2000) *J. Pharmacol. Exp. Ther.* **295**, 302–308
- Burchardt, T., Burchardt, M., Chen, M. W., Cao, Y., de la Taille, A., Shabsigh, A., Hayek, O., Dorai, T., and Buttyan, R. (1999) *J. Urol.* **162**, 1800–1805
- Bijlenga, P., Liu, J. H., Espinos, E., Haeggeli, C. A., Fischer-Lougheed, J., Bader, C. R., and Bernheim, L. (2000) *Proc. Natl. Acad. Sci. U. S. A.* **97**, 7627–7632
- Day, M. L., Johnson, M. H., and Cook, D. I. (1998) *Pflugers Arch.* **436**, 834–842
- Kuga, T., Kobayashi, S., Hirakawa, Y., Kanaide, H., and Takeshita, A. (1996) *Circ. Res.* **79**, 14–19
- Xu, X. P., and Best, P. M. (1990) *Proc. Natl. Acad. Sci. U. S. A.* **87**, 4655–4659
- Wang, Z., Estacion, M., and Mordan, L. J. (1993) *Am. J. Physiol.* **265**, C1239–C1246
- Chemin, J., Monteil, A., Briquaire, C., Richard, S., Perez-Reyes, E., Nargeot, J., and Lory, P. (2000) *FEBS Lett.* **478**, 166–172
- Berridge, M. J., Bootman, M. D., and Lipp, P. (1998) *Nature* **395**, 645–648
- Skryma, R., Mariot, P., Bourhis, X. L., Coppenolle, F. V., Shuba, Y., Abeele, F. V., Legrand, G., Humez, S., Boilly, B., and Prevarskaya, N. (2000) *J. Physiol.* **527**, 71–83
- Wang, L., Bhattacharjee, A., Zuo, Z., Hu, F., Honkanen, R. E., Berggren, P. O., and Li, M. (1999) *Endocrinology* **140**, 1200–1204
- Sculptoreanu, A., Abramovici, H., Abdullah, A. A., Bibikova, A., Panet-Raymond, V., Frankel, D., Schipper, H. M., Pinsky, L., and Trifiro, M. A. (2000) *Mol. Cell Biochem.* **203**, 23–31
- Lukyanetz, E. A., and Neher, E. (1999) *Eur. J. Neurosci.* **11**, 2865–2873
- Mansvelder, H. D., and Kits, K. S. (2000) *J. Physiol.* **526**, 327–339